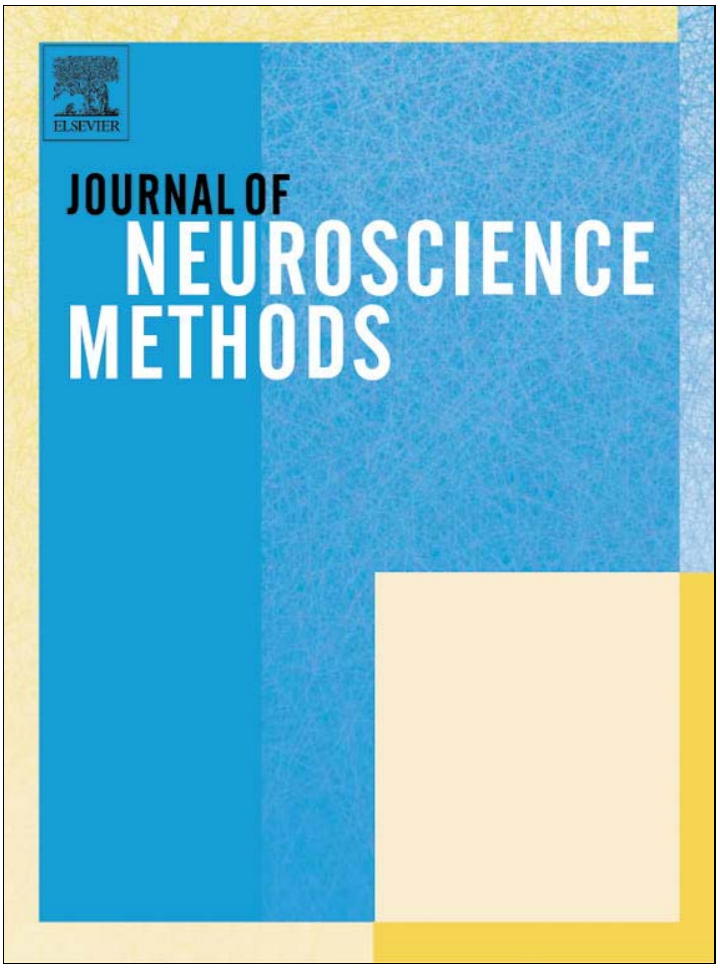

Journal of Neuroscience Methods 215 (2013) 121–131

Contents lists available at SciVerse ScienceDirect

Journal of Neuroscience Methods

journal homepage: www.elsevier.com/locate/jneumeth

Basic Neuroscience

Structural and quantitative neuroimaging of the common marmoset monkey using a clinical MRI system

Gunther Helms[a,*], Enrique Garea-Rodriguez[b], Christina Schlumbohm[c], Jessica König[b,d], Peter Dechent[a], Eberhard Fuchs[b,d], Melanie Wilke[a,d]

[a] Göttingen University Medical Center, Department of Cognitive Neurology, Göttingen, Germany
[b] German Primate Center, Clinical Neurobiology Laboratory, Göttingen, Germany
[c] Encepharm GmbH, Göttingen, Germany
[d] Center for Nanoscale Microscopy and Molecular Physiology of the Brain (CNMPB), University of Göttingen, Göttingen, Germany

HIGHLIGHTS

- Structural and quantitative MRI techniques transferred from humans to common marmoset monkeys on a clinical 3T scanner.
- T1-w and T2-w MRI and multi-parametric mapping can be run under injection anesthesia at 0.4 mm resolution.
- Cortical layers and axon-rich areas can be seen on magnetization transfer (MT) and T1 maps at 0.33 mm resolution.
- T1 and MT were comparable to humans, but smaller R2* in basal ganglia indicated lower iron content in marmosets.
- A disease model (experimental autoimmune encephalomyelitis) and dynamic mapping of contrast agent excretion are presented.

ARTICLE INFO

Article history:
Received 18 September 2012
Received in revised form 19 January 2013
Accepted 14 February 2013

Keywords:
Common marmoset
Translational studies
Experimental autoimmune encephalomyelitis
Quantitative magnetic resonance imaging
Gadolinium

ABSTRACT

Purpose was to adapt structural and quantitative magnetic resonance imaging (MRI) from humans to common marmoset monkeys on a clinical 3T scanner and to demonstrate the value for translational research.

Three-dimensional T1- and T2-weighted MRI and gradient echo-based multi-parameter mapping was performed on nine adult animals using a wrist coil. Structural MRI was applied in a model of targeted experimental autoimmune encephalomyelitis (EAE). Magnetization transfer (MT) and T1 parameter maps were used to depict axon-rich cortical areas. After intraveneous triple dose of gadobutrol, the excretion half-time was determined from consecutive measurements of R1 = 1/T1. Diffusion tensor imaging (DTI) was performed at 1 mm resolution.

At 0.4 mm resolution, total measurement time (30 min) was compatible with injection anesthesia, permitting rapid screening and frequent follow-up. Structural MRI depicted the EAE lesion in white matter. Quantitative values of T1, MT, and R2* in marmoset brain were comparable to humans, except for smaller R2* indicating lower iron content in basal ganglia. The middle temporal V5 area and the cortical layer IV could be identified, but were considerably better delineated when averaging two images at 0.33 mm resolution (70 min). A similar distribution volume (23%), but a shorter excretion half time than in humans (30 min) was observed. DTI was feasible only in larger structures, such as major axonal tracts.

High-resolution MRI of common marmosets proved feasible using clinical MRI hardware. A rapid 3D examination protocol was established for screening under injection anesthesia, thus avoiding the adverse effects of inhalation anesthesia.

1. Introduction

The common marmoset monkey (*Callithrix jacchus*) is a small-bodied new world primate. It is increasingly used as a model for human neurodegenerative diseases, e.g., multiple sclerosis (Merkler et al., 2006b), optic neuritis (Diem et al., 2008), and Parkinson's disease (Kirik et al., 2003; van Vliet et al., 2008). Non-invasive imaging techniques, such as magnetic resonance imaging (MRI) are

* Corresponding author at: Universitätsmedizin Göttingen, Abteilung Kognitive Neurologie, MRT4, TL190, Robert-Koch-Str. 40, D-37075 Göttingen, Germany. Tel.: +49 551 39 13132; fax: +49 551 39 13243.
E-mail address: ghelms@gwdg.de (G. Helms).

0165-0270/$ – see front matter © 2013 Elsevier B.V. All rights reserved.
http://dx.doi.org/10.1016/j.jneumeth.2013.02.011

mandatory for longitudinal studies in these disease models, particularly when potential therapies are tested. MRI provides a strong intrinsic contrast between gray and white matter (GM/WM) with a high sensitivity to atrophy, inflammation, and demyelination. Therefore, MRI is the method of choice to study models of white matter degeneration.

Dedicated MRI protocols to monitor disease progression or treatment in marmoset monkeys have been developed on small animal MRI systems (Bihel et al., 2010; Blezer et al., 2007; Boretius et al., 2006). Such protocols usually comprise a range of different diagnostic techniques. Structural T1-w(eighted) MRI provides the anatomical reference for spatial normalization and voxel-based morphometric analysis and the extravasation of gadolinium-based contrast agents. The diagnostic hallmark of T2-w MRI is its sensitivity to free water, which can be used to detect inflammation and demyelination of WM. In contrast to generic MR images that exhibit arbitrary signal strength, quantitative MRI techniques provide so-called parameter maps. Their values can be compared to healthy controls and followed-up in serial studies (Tofts, 2005). Parameter maps are more closely related to the micro-structural properties of tissue than the contrast of MR images. The longitudinal relaxation time (T1) is correlated to macromolecular content and can be manipulated by paramagnetic relaxation agents, such as gadolinium or manganese (Bock et al., 2009). The effective transversal relaxation time (T2*) is sensitive to axonal fiber density (Sati et al., 2012) and iron aggregates, like ferritin or super-paramagnetic contrast agents. Magnetization transfer (MT) contrast is solely based on the presence of macromolecules, particularly those of myelin. Diffusion tensor imaging (DTI) assesses the main direction and coherence of axons in WM.

The use of standard clinical MRI systems for common marmosets is highly desirable for researchers without access to a small animal MRI scanner that requires considerable investment and running costs. Moreover, translational research is often performed in a clinical environment, which may grant access to clinical MRI scanners. Small animal MRI scanners have clear advantages over clinical MRI systems, like a higher static magnetic field (B0), stronger magnetic field gradients and customized radio-frequency (RF) coils. Thus, they can provide a higher image resolution at a sufficient signal-to-noise ratio (SNR). However, special hardware may be needed to study marmosets because their brain is significantly larger than that of rats or mice. One advantage of using the same clinical scanner for studies of animal models and human disease is the comparability since contrast parameters and relaxivities depend on B0.

Thus, in order to facilitate clinical translational studies, we aimed to adapt neuroimaging protocols for humans to marmoset monkeys on a clinical 3T MRI system. We established a comprehensive protocol for structural and quantitative MRI at image resolutions commonly achieved in studies of disease models within clinically feasible measurement times ranging from 30 to 70 min. Initial applications in targeted EAE and kinetics of contrast agent, as well as a numerical comparison of relaxation parameter values to those observed in humans are presented.

2. Methods

Experiments were performed on a 3T clinical whole body MR system (Magnetom Tim Trio, Siemens Healthcare, Erlangen, Germany) using the standard body coil for RF transmission and an eight-channel wrist coil for signal reception (Invivo, Gainesville, FL, USA). The wrist coil was designed to accommodate the human carpus and palm and thus provided easy access from both ends.

2.1. Animal handling

A total of nine marmoset monkeys (5 females, 4 males, 3–10 years, 350–550 g) were scanned under general anesthesia. The effect of intramuscular injection anesthesia lasted about 30 min [(0.3 mg/kg diazepam, 10 mg/kg alphaxalon (Alphaxan®; Vetoqinol, Ravensburg, Germany), and 0.01 mg glycopyrronium-bromide per animal (Robinul®; Riemser Arzneimittel, Greifswald, Germany)]. For a 15–30 min extension of anesthesia, 0.05 ml of 10% ketamine solution (Ketamin Gräub, aniMedica GmbH, Senden, Germany) were injected after 30 min. In four animals, the anesthesia was extended with an inhalation anesthesia [60:40 N_2O:O_2; isoflurane (0.5–1.5%)] delivered by a respirator (TSE-Animal Respirator, TSE, Bad Homburg, Germany) via an intratracheal tube. Pulse frequency and blood oxygenation were monitored continuously using MRI-compatible equipment (Datex-Ohmeda, GE Healthcare, Helsinki, Finland).

Animals were fettered by taping the forelegs and scanned in supine position. The head was placed in carpal section of the wrist coil (2 cm proximal of the coil center) and padded without further fixation. At an ambient temperature of 21 °C, body temperature was maintained during the scan by wrapping the body and lower extremities in a soft towel. Under inhalation anesthesia, an additional heat reservoir was provided by water bottles at 36 °C. During preparation and recovery, animals were kept on temperature regulated heating pads.

The gadolinium-based MRI contrast agent gadobutrol (Gadovist®; Bayer Schering Pharma, Berlin, Germany) was applied into the saphenous vein in triple dose proportional to body weight as compared to humans (0.3 mmol gadobutrol per kg).

In order to test for applicability of the method in translational studies, we scanned one animal that received a unilateral injection of proinflammatory cytokines into the border area between white and gray matter within the left hemisphere and phosphate buffered saline (PBS) into the right hemisphere. The local inflammation was induced as described by Merkler et al. (2006a) with the following modifications: The animal was sensitized with 25 μg of recombinant rat myelin oligodendrocyte glycoprotein (MOG), solved in PBS and emulsified in incomplete Freund's adjuvants (IFA). Four subcutaneous injections (150 μL each) were placed in the shoulder and the loin region. A stereotactic injection with proinflammatory cytokines was carried out 43 days later. Injection volume was 2 μL (active agent and vehicle, respectively) per site. Injections were positioned 3 mm rostral and 3 mm temporal from bregma. The depth of injection was 3.5 mm below the pial surface. The animal was scanned on day 4 and day 17 after cytokine application under injection anesthesia.

All animals were obtained from the breeding colony at the German Primate Center (Göttingen, Germany) and from Encepharm (Göttingen, Germany). The animal experiments were approved by the Lower Saxony Federal State Office for Consumer Protection and Food Safety (LAVES) in accordance with German legislation on animal rights and welfare and the European Communities Council Directive of November 24, 1986 (86/EEC). The study was also carried out in line with the "Principles of Laboratory Animal Care" (NIH Publication no. 85-23, revised 1985).

2.2. MRI pulse sequences and parameter adjustments

Imaging volumes were acquired with three-dimensional (3D) spatial encoding, because the slice thickness in 2D MRI (≥0.9 mm) was considered insufficient. The imaging slab with a field-of-view (FoV) between 102 mm and 128 mm was oriented along the body axis of the animal, yielding axial-oblique slices. A FoV of about 50 mm in left-right and ventral-dorsal directions was sufficient to

Table 1
MRI protocols and sequence parameters.

Contrast	Sequence	Matrix[a]	Time[b]	TR/TE/TI/α[c]	BW[d]	pF
0.5 mm						
T1-w	MP-RAGE	256 × 104 × 96	3:26	2250/3.8/900/9°	200	7/8
T2-w	TSE	192 × 96 × 96	4:28	2900/271/–/vfl[e]	357	7/8
PD-w	FLASH	256 × 96 × 96	2:37	30/14.7/–/5°	300	6/8
T1-w	FLASH	256 × 96 × 96	2:37	30/14.7/–/28°	300	6/8
0.4 mm			25:00			
T1-w	MP-RAGE	320 × 130 × 120	4:18	2250/4.0/900/9°	200	7/8
T2-w	TSE	256 × 128 × 120	5:26	2900/278/–/vfl	355	7/8
PD-w	FLASH	320 × 120 × 120	4:05	30/14.7/–/5°	300	6/8
T1-w	FLASH	320 × 120 × 120	4:05	30/14.7/–/28°	300	6/8
MT-w	FLASH	320 × 120 × 120	6:06	45/14.7/–/11°	300	6/8
0.33 mm			66:04			
T1-w	MP-RAGE	384 × 156 × 144	5:10	2250/4.3/900/9°	200	7/8
T2-w	TSE	320 × 152 × 144	6:48	2900/272/–/vfl	355	7/8
PD-w	FLASH	384 × 144 × 144	6:03	31/14.7/–/5°	310	6/8
T1-w	FLASH	384 × 144 × 144	6:03	31/14.7/–/28°	310	6/8
MT-w	FLASH	384 × 144 × 144	8:58	46/14.7/–/11°	310	6/8

[a] Given for read × phase × slice directions. The corresponding FoVs can be calculated from matrix dimension and resolution.
[b] Given as min:s.
[c] In units of [ms]/[ms]/[ms]/°. Effective TE values are given for multiple TEs.
[d] In units of Hz/pixel.
[e] vfl = variable refocusing flip angles.

avoid fold-over at the head (with the ears being placed close to the skull).

For structural MRI with T1-w contrast, a magnetization-prepared rapid acquisition of gradient echoes (MP-RAGE) sequence was used with the parameters recommended in Jack et al. (2008) (inversion time TI = 0.9 s, read-out flip angle $\alpha = 9°$, repetition time TR = 2.25 s, bandwidth BW = 200 Hz/px).

T2-w MRI was performed using turbo spin-echo (TSE) sequences with variable refocusing flip angles (2 averages with phase partial Fourier, slice turbo factor 2, GRAPPA (general autocalibration for parallel partial acquisition) factor 2 with 24 reference lines).

Quantitative MRI of relaxation parameters (multi-parameter mapping) was based on the fast-low angle shot (FLASH) technique with read-out of multiple gradient echoes as described in human brain studies (Gringel et al., 2009; Helms et al., 2008a; Helms and Dechent, 2009). The TR of 30 ms (Helms et al., 2008a) accommodated seven equidistant gradient echoes at echo times (TE) of 3.69, 7.38, ... and 25.83 ms. At these TE, the phase of water and lipid signals alternates between 180° and 0°. In brain tissue, where free lipid signals are absent, regression of the logarithmized echo signals yielded the effective T2-relaxation rate, $R2^* = 1/T2^*$.

In three different acquisitions, FLASH images with predominant proton density (PD), T1, and MT weighting were acquired. The averaged echo signals were transformed into parameter maps of T1-relaxation time (sensitive to gadolinium-based contrast agents), effective T2 relaxation rate (sensitive to tissue iron) and MT saturation (Helms et al., 2008b) for an improved contrast of the deep brain nuclei (Helms et al., 2009). Contrary to human studies, the T1 maps needed no correction for flip angle inhomogeneity because the marmoset head is much smaller than the RF wavelength at 3T (about 25 cm).

The MRI protocols at different isotropic resolution are detailed in Table 1. The parameter settings were based on the following experiments.

2.3. Experiment 1: image resolution

To assess the trade-off between image noise, anatomical detail, and measurement time, T1-w and T2-w MRI was performed at 0.5 mm, 0.4 mm, and 0.33 mm isotropic resolution. The MRI scanner imposed minor alterations in sequence timing. The bandwidth was kept constant at 200 Hz/pixel and 355 Hz/pixel for T1-w and T2-w MRI, respectively. The increase of the matrix size (Table 1) prolonged the measurement time, as well as the read-out train of spoiled gradient echoes and spin echoes of the MP-RAGE (96 to 120 to 144) and TSE sequences (630 to 726 to 846), respectively.

To analyze the dependence of SNR and contrast-to-noise ratio (CNR) for different resolutions, circular ROIs of 2 mm diameter were placed in the caudate head and adjacent frontal WM, comprising 33, 81, and 123 pixels, respectively. The standard deviation of image noise was determined from the root mean squared (rms) signal of a 12 mm ROI placed in air (Constantinides et al., 1997). For "noise", we refer to the combined noise of the eight coil elements. This relates approximately to the $sqrt(2/\pi)$ of the mean noise "floor" of the rms combined signal, thus facilitating the comparison between coils with a different number of coils elements.

2.4. Experiment 2: targeted EAE

One day before the stereotactic application of cytokines, a baseline scan was performed. The effect of cytokine application was studied 4 days and 17 days after the intracerebral application. In addition, 3D FLAIR MRI (fluid attenuation by inversion recovery, TI = 1.8 s, TR = 5.5 s) was acquired after intravenous gadobutrol application on day 4.

2.5. Experiment 3: flip angle optimization of multi-parameter mapping

To optimize the SNR in the parameter maps, the flip angle of each FLASH acquisition (α_{PD}, α_{T1}, and α_{MT}, respectively) was adjusted to account for putative differences between marmosets and humans. The optimal settings refer to the Ernst angle (α_E) – that is, the local flip angle that would produce the maximum FLASH signal at a given TR – by $\alpha_{PD} = \alpha_E/(1+\sqrt{2})$ and $\alpha_{T1} = \alpha_E(1+\sqrt{2})$, respectively (Dathe and Helms, 2010). For the MT-w FLASH with an additional MT-pulse, $\alpha_{MT} = \alpha_E^{MT}/\sqrt{3}$ minimizes noise progression into the MT maps (Gringel et al., 2009). For both scenarios, maps of the apparent T1 rates were estimated by dual-angle experiments and converted into maps of α_E in units of degrees by the approximate equation $\alpha_E = sqrt(2\,TR/T1)180°/\pi$ (Helms et al., 2008a). Choice of flip angles was based on the median Ernst angle of brain tissue.

2.6. Experiment 4: cortical parcellation by multi-parameter mapping

Finally, the 0.4 mm and 0.33 mm protocols were checked for consistency in respect to quantitative values and anatomical detail in 4 animals. For this purpose, regions-of-interest (ROIs) were selected manually in the splenium of the corpus callosum, the head of the caudate nucleus and the ventricles. These structures are representative for GM, WM, and cerebro-spinal fluid (CSF), respectively. In addition, ROIs in the globus pallidus and the visual area of the mesio-temporal lobe ("MT"/V5) were chosen to target iron-rich GM and myelin-rich cortex.

2.7. Experiment 5: excretion of contrast agent by R1 mapping

The excretion of the contrast agent gadobutrol was monitored up for about 35 min in one female marmoset monkey (body weight 516 g). The longitudinal relaxation rate R1 = 1/T1 is directly related to the average concentration of contrast agent [CA] in the voxel by the equation $R1 = r_{1CA}[CA] + R1b$. Here, r_{1CA} is the specific relaxivity of gadobutrol, which has been determined to be $3.6 \pm 0.2\,l\,s^{-1}\,mmol^{-1}$ in plasma at 37 °C and 3T (Pintaske et al., 2006).

The baseline relaxation rate R1b at baseline was calculated from the averaged PD-w and T1-w multi-echo FLASH data at 0.4 mm resolution. After receiving an intravenous dose of 0.15 mmol/kg gadobutrol and an intramuscular injection of 0.05 ml ketamine 10% (see above), consecutive estimates of R1 were calculated from PD-w and T1-w FLASH at a spatial resolution of 0.5 mm (2× 2:36 min). R1 in venous blood was determined from a ROI placed in the straight sinus on the T2-w volume. Starting concentration, time constant of excretion, and baseline were then estimated by fitting an exponential transition to the time points.

2.8. Experiment 6: diffusion tensor imaging

Diffusion tensor imaging (DTI) was performed on contiguous untilted "axial" slices of 1 mm thickness and 98 mm FoV with echo-planar imaging (EPI). Phase encoding was in the "anterior-posterior" direction with a 74 mm FoV (75%). Here, the nominal orientations as displayed on the console, are indicated by quotation marks. In order to constrain TE to a minimum value of 91 ms (yielding a TR of 4 s for 30 slices), a GRAPPA factor 2 with 16 reference lines and a maximum *b*-value of 800 s/mm^2 was applied. In addition to an isotropic scheme of 64 diffusion directions at 800 s/mm^2 (4:34 min), a very low diffusion weighting ($b = 50$ s/mm^2) was applied along 6 diffusion directions to serve as additional references (0:38 min). The diffusion tensor was calculated off-line as described below.

2.9. Data processing and display

Data processing was scripted using routines of the FSL 4.1 software library of the Centre for Functional Magnetic Resonance Imaging of the Brain (FMRIB, University of Oxford, UK, www.fmrib.ox.ac.uk/fsl). The axial oblique DICOM images (digital imaging and communications in medicine) in the radiological right-left convention were converted to 3D NIFTI volumes (neuroimaging informatics technology initiative) following the neuroscience left-right convention. The T1-w volume was aligned to the intercommissural orientation [as in used in Yuasa et al., 2010 and in human stereotaxis], interpolated to 0.25 mm by registration to a custom-made marmoset head template using the FSL linear registration tool (FLIRT, 6 parameter rigid body transform). The T1-w volume then served as an individual reference for aligning the other data sets. Maps of R2* were calculated by log-regression; maps of the signal amplitude A, T1, and MT saturation were calculated as described in Gringel et al. (2009). The frequency of estimated T1, R2*, and MT values in the brain were determined by histogram analysis using FSLview. The MRIcro freeware was used to create color overlays, for ROI placement and analysis (http://www.cabiatl.com/mricro/mricro/index.html).

The DTI multi-slice ("mosaic") images were converted into volumes in the generic radiological representation of the gradient coordinate system. The diffusion tensor was then fitted using the FSL diffusion tool (FDT) and the diffusion directions specified in gradient space. Evaluation was performed across a mask comprising the brain and the eyes. In a second step, the diffusion parameter maps were re-ordered using the "fslswapdim" command prior to co-registration to the T1-w anatomical reference.

3. Results

The human wrist coil offered ample space for the head and chest of the marmosets. The sensitive region of the coil covered the whole head and neck of the animals. The brain areas that were located closest to the coils, namely parietal and occipital cortex, showed a moderately higher signal than the remaining brain. Nevertheless, the whole MRI volume could be viewed without readjustment of the gray scale window.

Since the marmoset brain is rotated by 90° with respect to the standard orientation of a human brain, "coronal" orientation was chosen in order to obtain axial views of the marmoset brain. In general, examinations at a resolution of 0.4 mm were compatible with the time constraints of anesthesia by intramuscular injection. With inhalation anesthesia and thus more time for data acquisition, 0.33 mm resolution was achieved.

3.1. Experiment 1: image resolution

The effect of decreasing the voxel size is demonstrated in a transversal slice at the level of the superior colliculi (Fig. 1). This slice contains also the occipital cortex, major deep brain structures (thalamus, caudate head, and anterior putamen), and a section through the posterior hippocampus, the straight sinus, and various CSF spaces.

At a resolution of 0.5 mm, tenuous CSF structures appeared blurred by partial volume effects, whereas 0.33 mm resolution resulted in poor SNR. At 0.33 mm resolution, noise reduction was achieved by averaging two acquisitions, revealing more anatomical detail in the deeper structures (such as the habenulae and CSF spaces) and within the cortex. The T2-w images resolved the highly myelinated cortical layer IV in some regions, which was best seen in area V1 (stria of Gennari). However, cortical layers could not be resolved on the corresponding T1-w structural images. If one is not interested in resolving specific layers, an isotropic resolution of 0.4 mm without averaging offered an acceptable compromise between SNR and anatomical detail.

The TSE images showed more blurring in the phase encoding left-right direction than in the anterior-posterior read direction. This could be seen by comparing the appearance of the tenuous band of WM between putamen and the lateral sulcus on T1-w and T2w MRI. The point spread-function of the TSE images has been broadened by variable refocusing flip angles and by the combination of partial Fourier and parallel acquisition.

In general, TSE offered higher SNR but less contrast than MP-RAGE. At 0.5 mm resolution, the residual fat signals of the posterior scalp appeared shifted toward the occipital cortex. Note that the T2-w signal of parenchyma and the signal of subcutaneous fat decreased with increasing resolution, due to longer acquisition trains. This also lead to a reduction in contrast between GM and WM

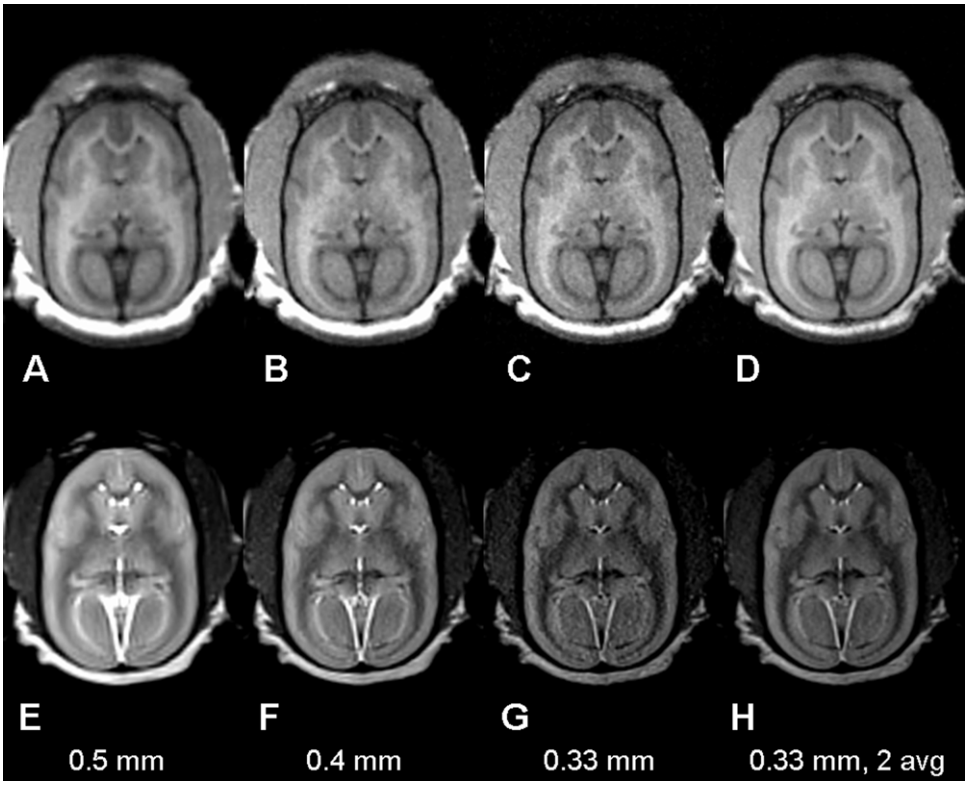

Fig. 1. Conventional MRI at different resolution. Top row: MP-RAGE at 0.5 mm (A), 0.4 mm (B), and 0.33 mm resolution (C). Bottom row: TSE at 0.5 mm (E), 0.4 mm (F), and 0.33 mm resolution (G). The right panels (D and H) show the average of two 0.33 mm images featuring increased SNR and improved anatomical detail. The gray-scale windowing is chosen identical within the rows to display variations in image intensity.

for higher resolution (41% to 36% to 33% for MP-RAGE and 26% to 25% to 23% for TSE). When increasing the resolution from 0.5 mm to 0.4 mm to 0.33 mm, the SNR the caudate head decreased from 16.0 to 12.0 to 9.4 and from 117.5 to 65.4 to 36.2 for MP-RAGE and TSE, respectively. After averaging two datasets, the choice of 0.33 mm resolution implied only a minor loss in the WM-GM contrast-to-noise ratio when compared to the 0.4 mm protocol (5.3 vs. 5.4 for MP-RAGE and 10.5 vs. 14.1 for TSE).

3.2. Experiment 2: targeted EAE

T2-w MRI revealed a unilateral hyperintense lesion at day 4 after intracerebral cytokine application, whereas the opposite hemisphere remained unaffected (Fig. 2, top row). The lesion appeared hypointense on T1-w MP-RAGE (Fig. 2, middle row), but did not show extravasation of gadobutrol (Fig. 2, bottom row). Dural contrast enhancement was seen in both surgical lesions. In view of the tenuous ventricular spaces, 3D FLAIR (not shown) yielded only small benefits over TSE at the cost of longer measurement time and lower SNR. By day 17, the contrast changes had reverted to baseline (Fig. 2, right column), indicating abatement of the inflammation (confirmed by histology, data not shown), as well as recovery processed after surgery.

3.3. Experiment 3: flip angle optimization of multi-parameter mapping

Since the animals were very small compared to a human body, the RF body coil did operate under a nearly unloaded and thus reproducible conditions. The transmitter reference voltage that determined the flip angle varied between 366 V and 392 V (mean ± SD 380.0 ± 7.5 V). The scan-rescan deviation was about 1% indicating highly reproducible flip angles. Without MT-pulse, the Ernst angles (Fig. 3A) depend directly on the local T1 values. The histogram showed a trimodal distribution with a 12° median value (Fig. 3B, for T1 see Fig. 4A). This value corresponded to GM, coded green in Fig. 3A. Hence, flip angles of 5° and 28° were chosen to minimize noise propagation for dual angle T1-mapping. Larger Ernst angles (yellow to red) were observed in WM and deep brain, while smaller values (indigo to black) were found in the hippocampus (not shown) and in CSF. A somewhat higher noise is expected in these tissues, where the chosen flip angles did not match the local Ernst angle. In the MT-FLASH experiment, the apparent rate of T1 relaxation was increased by a tissue dependent contribution of δ_{MT}/TR. The combination of a shortened T1 and a longer TR of 45 ms yielded larger Ernst angles than without MT-pulse (Fig. 3C). These Ermst angles showed a broadened unimodal distribution (Fig. 3D). The median value of 19° (observed in GM, green in Fig. 3C) corresponded to a flip angle of 11° to minimize propagation of error from the MT-w images into the MT-maps (Gringel et al., 2009).

3.4. Experiment 4: cortical parcellation by multi-parameter mapping

The parameter maps and whole-brain histograms are shown in Fig. 4. Values of T1, MT, and R2* are given in Table 2 for selected brain structures, together with data obtained in humans.

In the T1 distributions (Fig. 4, top row), the shortest T1 values represent fully myelinated WM (coded indigo). The underlying mode was much smaller than in humans (compare Fig. 4B of Helms et al., 2008a,b) and did not show a separate peak value, reflecting the reduced proportion of WM compared to GM in marmosets. In marmosets, an intermediate T1 mode around 1200 ms was revealed between GM and WM, which was not seen in humans. The corresponding signals were mainly found in the brainstem (less distinctly coded by a darkish hue between indigo and green) and

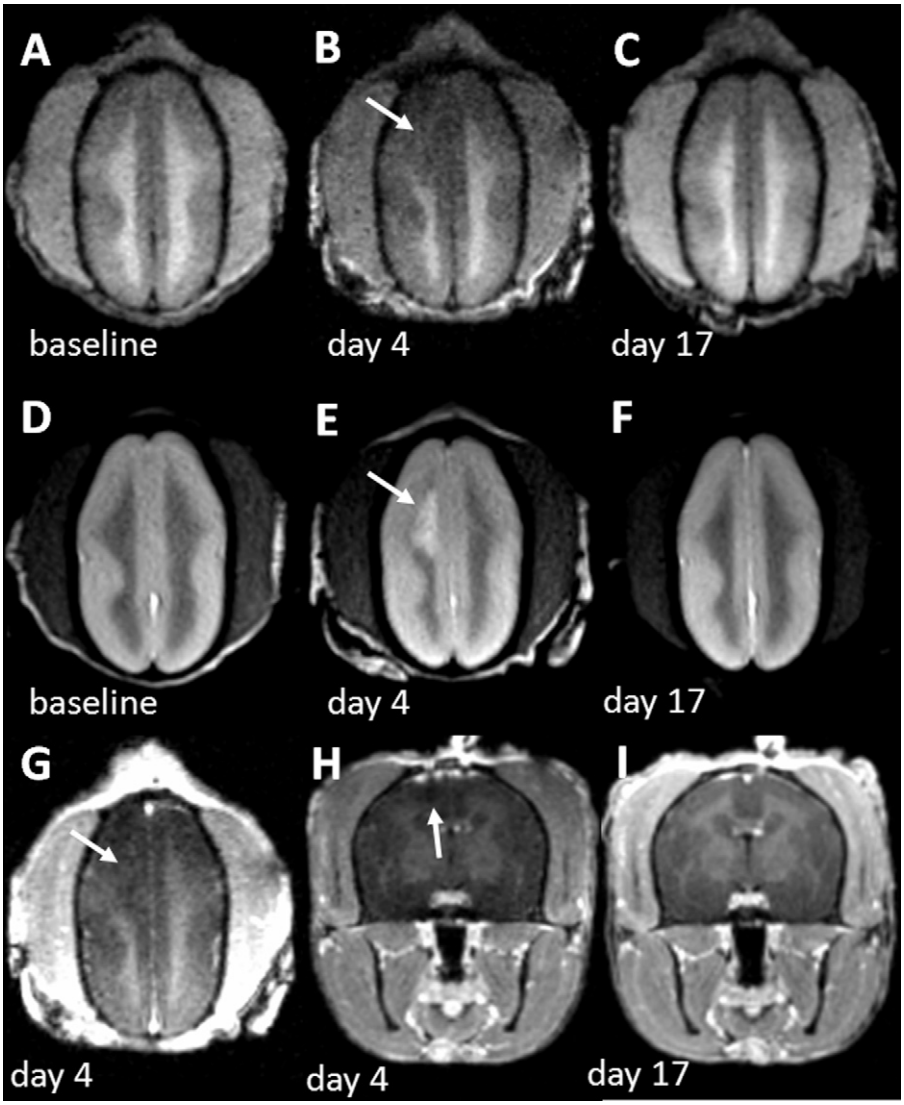

Fig. 2. Conventional MRI in targeted EAE. Images taken at baseline before (A and D), 4 days (middle column and G) and 17 days (right column) after stereotactic application of cytokines. Top row: T1-w MP-RAGE; middle row: T2-w TSE; bottom row: T1-w MP-RAGE after gadobutrol. Signs of inflammation (arrows), but no contrast enhancement, were visible on day 4. On day 17 the lesion had disappeared.

Table 2
Multi-parameter mapping.

	Splenium	Pallidum	Cortex V5	Caudate	Ventricle
Marmoset T1 [ms][a]	957 ± 48	993 ± 43	1245 ± 24	1358 ± 41	3202 ± 505
Human T1 [ms][b]	773 ± 71[c]	970 ± 66[c]	1441 ± 32[d,f]	1277 ± 94[c]	4619 ± 893[e]
	1072 ± 80[d]	987 ± 53[e]		1278 ± 80[e]	5664 ± 597[d]
R2* [1/s][a]	24.4 ± 4.0	23.7 ± 2.7	18.7 ± 1.4	16.6 ± 1.4	7.8 ± 5.1
Human[b]	22.1 ± 3.4[c]	34.5 ± 2.5[c]	n.d.	22.0 ± 2.5[c]	1.9 ± 0.9[e]
		37.6 ± 5.5[e]		19.8 ± 2.2[e]	
MT [%][a]	4.47 ± 0.27	3.10 ± 0.16	3.14 ± 0.16	2.39 ± 0.16	0.31 ± 0.11
Human[b]	4.53 ± 0.32[e]	3.48 ± 0.19[e]	n.d.	2.62 ± 0.18[e]	0.31 ± 0.07[e]
ΔT1 [%][g]	−6.1 ± 3.8	−7.2 ± 3.7	−5.4 ± 2.4	−7.9 ± 1.5	−82 ± 59

[a] Values given a mean ± SD of 6 animals.
[b] Data from previous studies in humans are given for comparison:
[c] From Helms and Dechent (2009).
[d] From Helms et al. (2008a).
[e] From Gringel et al. (2009), partly unpublished.
[f] From occipital cortex V1.
[g] Percent changes after a triple dose of Gadovist® determined on 3 animals.

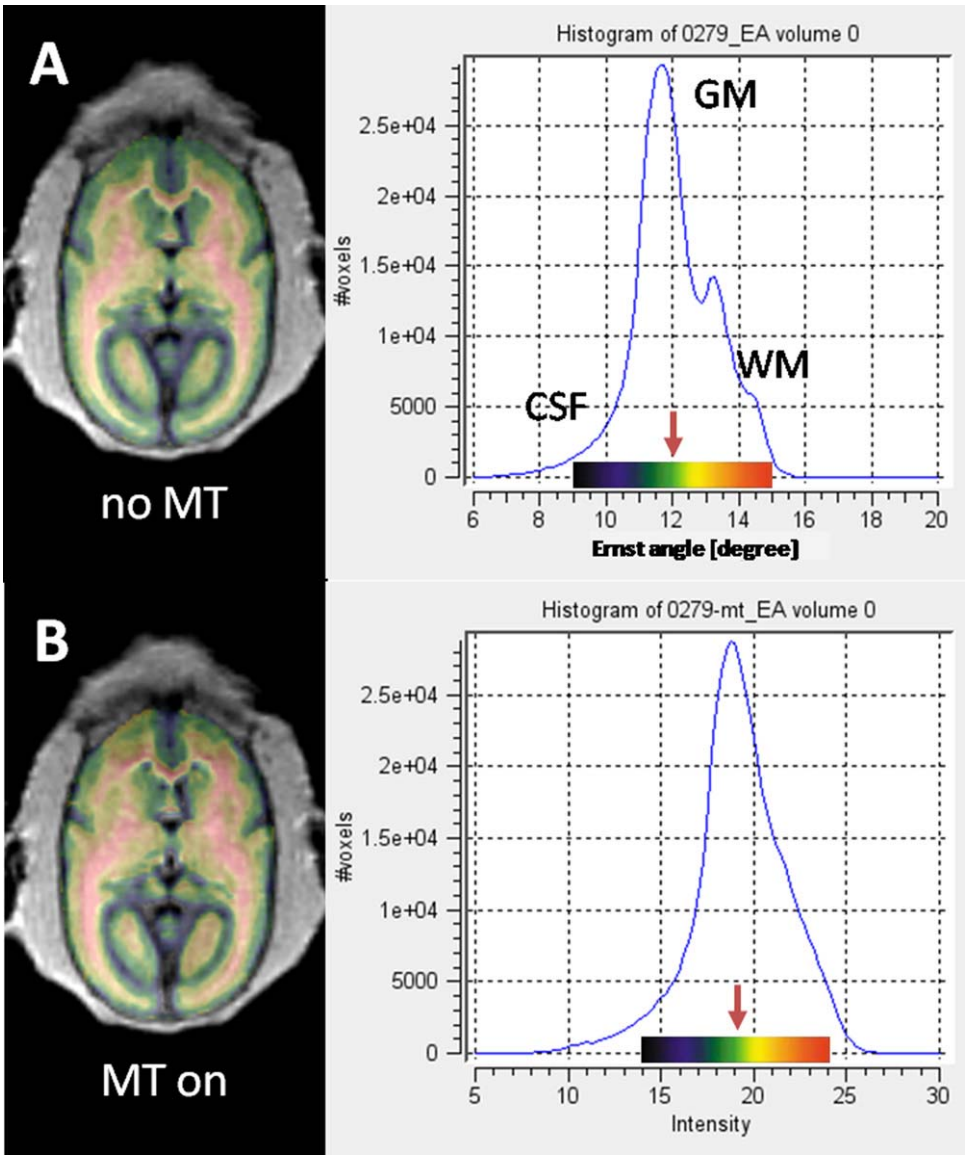

Fig. 3. Color display and histograms of the local Ernst angle. Dual-flip angle experiments were performed at TR = 30 ms without (A) and with MT pulse at TR = 45 ms (B). The arrows in the histograms indicate the median Ernst angle of brain parenchyma, used to determine the flip angles.

likely represent WM with interspersed nuclei. On the MT maps (Fig. 4, middle row), WM is represented by a separate mode of a peak value of 4.1 p.u. (coded red), reflecting the influence of myelin on MT. The GM mode comprises a broad range of greenish hues, with the lowest MT values found in the hippocampus. Values between the GM and WM peaks are coded yellow and likely represent a high content of myelinated axons in GM or partial volumes of WM and GM. They did not show a distinct mode like for T1.

On the coronal views of the T1 and MT maps, the middle temporal visual cortex (V5, white arrows), can be identified by the content of myelin in the deeper cortical layers (Bock et al., 2011). MT saturation maps yielded a larger percent difference between V5 and caudate (36 ± 8%) than T1 maps (28 ± 6%, $p < 0.001$, paired one-sided t-test). Here, 100% refer to the difference between splenium and caudate that represent typical structures of WM and GM, respectively. Intra-cortical structures such as the V5 area were better delineated at 0.33 mm (Fig. 4, middle column). At this higher resolution, even an intracortical layer was resolved (yellow arrows). From its small T1 and high MT values, it may be inferred that this is the axon-rich layer IV.

The R2* maps (Fig. 4, bottom row) showed an inferior SNR than the T1 and MT maps (even at 0.4 mm) and suffered from susceptibility artifacts in the ventral regions of the brain (coded red). These artifacts are caused by interfaces between brain, bone and air, but affect a proportionally larger area in marmosets than in humans. Accordingly, the R2* histograms showed a single mode of GM and WM and an extended "tail" representing the artifacts.

ROI analysis showed that, there were no significant systematic deviations between the parameter maps at different resolutions. The mean absolute deviations over all ROIs in parenchyma indicated that T1 maps were more reproducible than MT maps (2% for T1, 5% for MT). Least reproducible was R2* with an error of 12%.

3.5. *Experiment 5: excretion of contrast agent by R1 mapping*

The contrast agent was mainly taken up in vessels, muscle, and fatty tissues, but not into brain parenchyma (Fig. 5). The percent decrease of T1 (Table 2) was about the same in the splenium (6.1%) and in gray matter (5.4–7.9%). Thus, the contrast between GM and

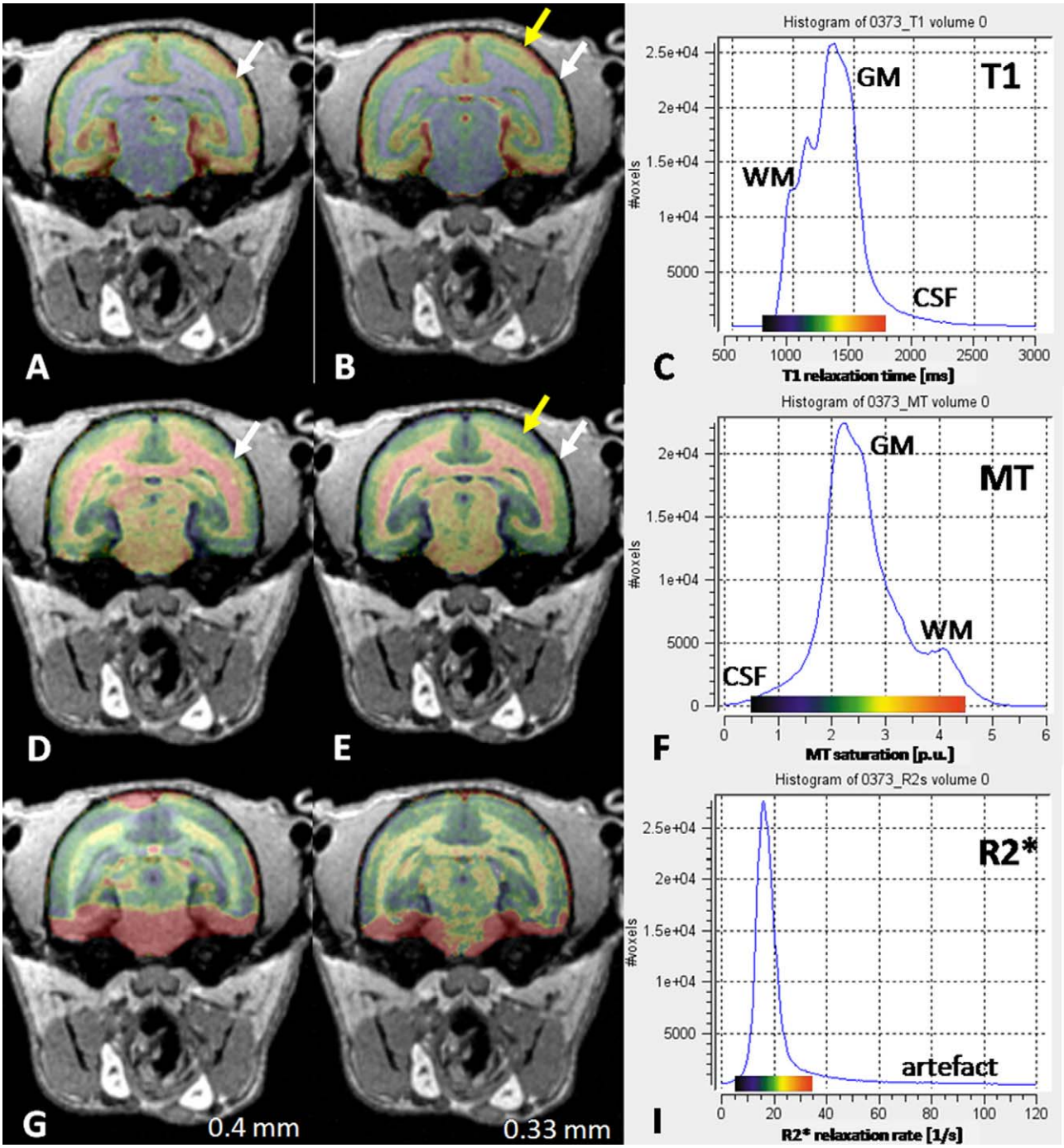

Fig. 4. Color display and histograms of parameter maps. Parameter maps derived from multi-echo FLASH at 0.4 mm (left column) and 0.33 mm resolution (middle column): T1 (top row), MT saturation (middle row), and R2* (bottom row). Mapping performed in the same animal under injection anesthesia (0.4 mm, 15 min) and under inhalation anesthesia (0.33 mm, 42 min). The parameter maps are displayed by a transparent pseudo-color overlay over the structural T1-w MRI. Color-coding is indicated by the bars in the histograms (right column). The coronal view runs through the V5 area (white arrows), splenium, hippocampus and pons. Intracortical structures like the axon-rich layer IV (yellow arrows) were not resolved at 0.4 mm. Note the appearance of a peak between GM and WM in the T1 histogram. This mode corresponds to the right shoulder of the GM mode in MT histogram. The red areas on the R2* maps show regions affected by B0 inhomogeneity (corresponding to the tail in the histogram at R2* > 35 1/s).

WM was only marginally reduced, with major vessels and meninges appearing clearly enhanced.

The half time of excretion (Fig. 5C) was 29.5 min (±1.0 min standard error). The increase of R1 in venous blood was $4.58 \pm 0.07\ s^{-1}$. This corresponds to an initial concentration of 1.27 mmol/l in blood, using the relaxivity determined by Pintaske et al. (2006). Thus, an estimate for the distribution volume of 0.23 l/kg is obtained (assuming instant equilibration of the applied dose of 0.29 mmol/kg across a non-exchanging compartment).

3.6. Experiment 6: diffusion tensor imaging

The selected untilted "axial" slices presented a upside-down coronal view of the marmoset brain. This orientation of the images was initially maintained in order to use the diffusion directions specified in gradient space for calculating the diffusion tensor. If the volumes are to be re-ordered to obtain the same orientation as from "coronal" slices prior to evaluation, the vector components of the diffusion directions have

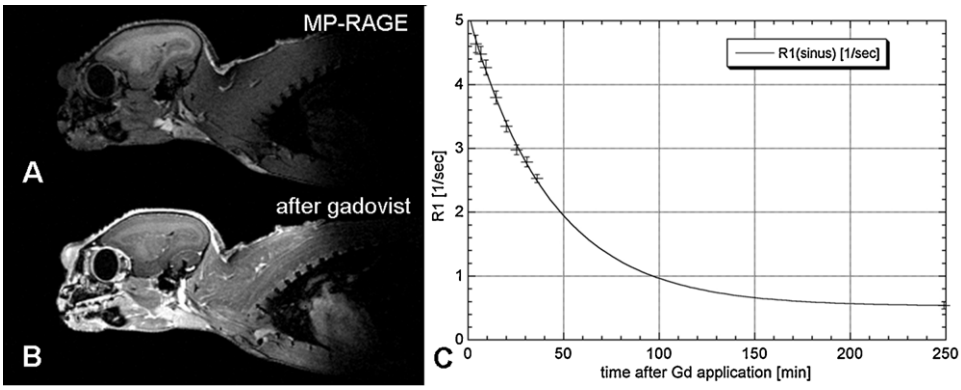

Fig. 5. Uptake and excretion of the contrast agent Gadovist®. Sagittal view of the original 0.4 mm MP-RAGE volume prior (A) and 8 min after (B) application of a triple dose of Gadovist®, shown at identical window settings. Vessels, fatty and muscle tissue appear enhanced, whereas the contrast in brain parenchyma is little affected. Note also the sensitive region of the wrist coil (about 90 mm). For curve fitting (C), the baseline measurement was assigned very long time. The error bars indicate the SD across the ROI.

to be submitted to the same operations (permutation and flipping).

The standard color-coding of the main diffusion direction in "axial" orientation at the generic image resolution is presented in Fig. 6A. To facilitate the assignment of underlying anatomical structures, the color map was superposed to the re-orientated T1-w volume. The transparency was modulated by the fractional anisotropy (FA). At 1 mm resolution, the pyramidal tracts and the optic radiation could still be resolved.

Histograms of the mean diffusivity (MD) and the FA are shown in Fig. 6B.The MD mode between 2.5 and 3 μm^2/ms represented bulbar fluid. In the FA histogram, however, width and peak value are larger than usually seen in humans, indicating the higher uncertainty in FA due to smaller voxel size and lower *b*-values. To illustrate the spatial congruence of the low-resolution EPI-based DTI with the high-resolution structural MRI, Fig. 6C shows the reordered FA map after affine transformation to the intercommissural orientation. The color bar is shown above the FA histogram. The transversal view through the splenium (white) is slightly more superior to that of Fig. 1. Distortions of symmetry were likely due to limitations of the affine spatial transformation. Despite an expansion in the superior-inferior direction, the residual spatial mismatch between the FA map and the anatomical images was of the order of 1 mm, as illustrated by the coronal slice containing

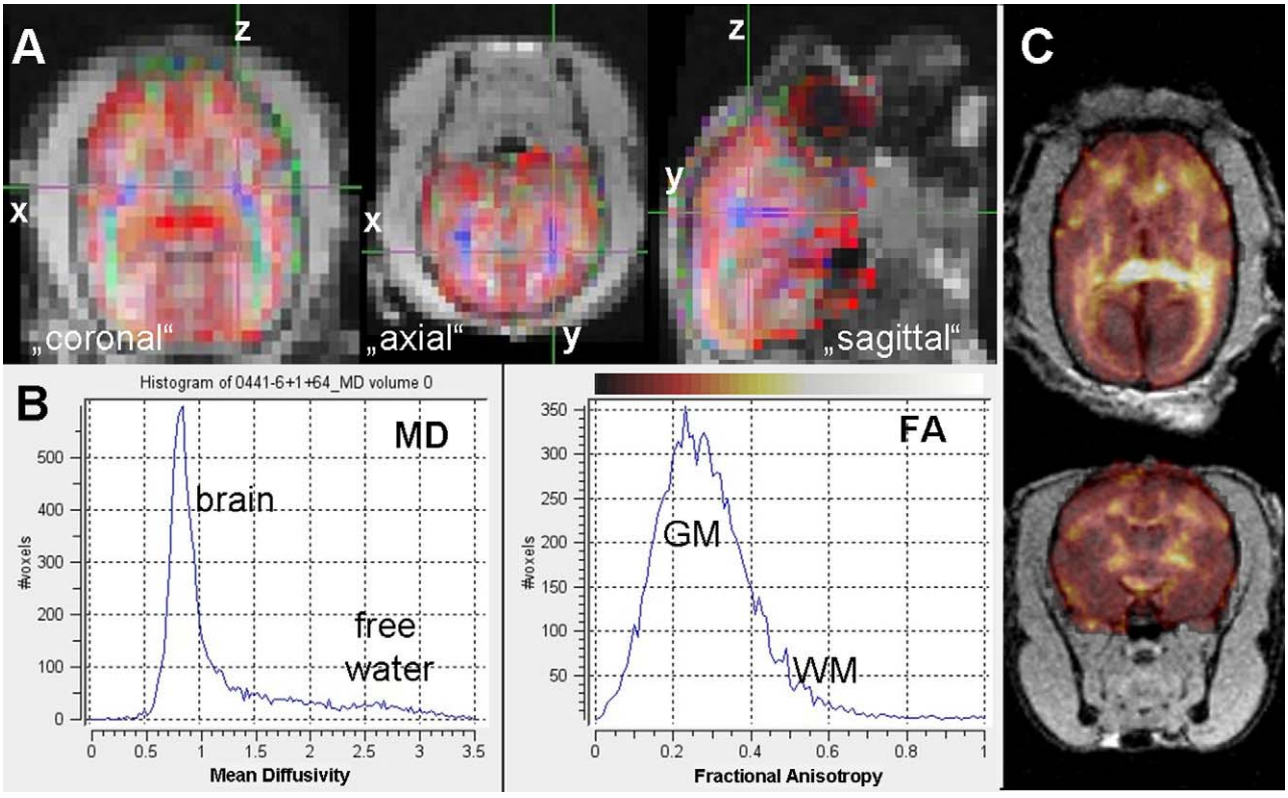

Fig. 6. Diffusion tensor imaging. Panel A shows the main diffusion direction derived from the generic images on three orthogonal views as displayed in FSLview. The gradient axes are labeled *x*, *y*, *z*. Viewing directions in quotation marks refer to human anatomy in supine-head first position and follow the radiological right-left convention. Note the rotation of coronal into axial views. For display purposes, the *y* and *z* components of the main diffusion direction were changed accordingly, in order to maintain consistency of the color channels with the use in human brain. Panel B shows the histograms of MD and FA across a mask covering brain and eyes. Panel C shows an opaque overlay of the FA map onto the MP-RAGE volume after left-right conversion and swapping *y* and *z*.

the anterior commissure. The highest FA values were observed in the splenium of the corpus callosum, but DTI was compromised by partial volume effects in the callosal body and the genu.

4. Discussion

Protocols for structural and quantitative MRI in humans were adapted for the study of marmoset monkeys on a 3T clinical MRI scanner with a standard human wrist coil. Although this coil is quite commonly used for small animal studies, this is the first report where it was applied as a head coil for marmoset monkeys. Anesthesia by intramuscular injection is well tolerated by the animals as it does not require intubation, but wears off after approximately half an hour. In the current study we show that within this time frame it is possible to perform either 3D structural T1-w and T2-w MRI at 0.33 mm isotropic resolution or a comprehensive examination at 0.4 mm resolution comprising 3D MRI and FLASH-based multi-parameter mapping. The rapid protocol designed for injection anesthesia represents an acceptable compromise between time, SNR, and anatomical detail. Since the adverse effects of supported respiration are avoided it can be used for routine screening of animals or in pre-clinical studies that require a frequent follow-up scans. The structural MP-RAGE can also be used to provide the anatomical correlates for functional molecular imaging at lower resolution, e.g., single photon emission computed tomography (Garea-Rodríguez et al., 2012).

3D MRI techniques with isotropic resolution were chosen, because this facilitates the alignment of volumes to a template (Hikishima et al., 2011). Thus, a consistent stereotaxic angulation, e.g., to the intercommisural line, can be achieved. Nevertheless the volumes can be easily transformed to other stereotaxic landmarks, e.g., bregma and intraaural line as in Palazzi and Bordier (2008). On the 3T scanner, DTI (Bihel et al., 2011; Yamada et al., 2008) is feasible at 1 mm resolution within the constraints of the gradient system, but the implementation is not straightforward. We have shown that problems related to orientation can be overcome, but the spatial congruence would benefit from non-linear distortion correction. The resolution proved sufficient to depict the major WM tracts. However, since finer anatomical details were blurred by partial volume effects and tensor-based tracking of tenuous WM fibers seemed not feasible, we opted against including DTI into the protocol for routine screening. Yet, it seems possible to monitor microstructural changes in WM lesions provided these are homogeneous and far larger than 1 mm (as shown in Fig. 2).

To date, studies in marmosets have mostly been performed on experimental MRI systems dedicated to small animals (Liu et al., 2011). Since such scanners typically operate at a higher magnetic field strength B0 than clinical scanners, both protocol design and translation of the results may have to take into account the influence of B0 on the relaxation times and, thus, image contrast. The main advantage of small animal MRI systems is that stronger gradients and higher field strength allow for thinner slices and higher spatial resolution. Nevertheless, on our 3T clinical MRI system we were able to perform quantitative mapping of multiple parameters at 0.33 mm resolution, thus surpassing the isotropic 0.6 mm recently reported for T1 mapping at 7T (Liu et al., 2011). This demonstrates the gain in SNR obtained by averaging multiple gradient echoes (Helms and Dechent, 2009). In addition to the initial setup of multi-echo FLASH protocols for human studies (Gringel et al., 2009; Helms et al., 2008a), the flip angles were determined by a qualified SNR optimization based on mapping of the local Ernst angle (Dathe and Helms, 2010). It should be noted, that a resolution below 0.33 mm (down to 0.11 mm) is technically feasible on the 3T MRI system, but this would require excessive averaging to recover the SNR.

For contrast enhancement, a triple dose of Gadovist® was injected as recommended in Blezer et al. (2007). The percent changes of T1 in GM at 3T were similar to those reported for gadopentate dimeglumin (Gd-DTPA) at 4.7T (Blezer et al., 2007). Gadobutrol and Gd-DTPA are renally filtered and excreted but not reabsorbed. Their disappearance from blood therefore mainly depends on glomerular filtration rate. The latter is proportional to metabolic body weight, which can roughly be calculated from body mass potentiated with 0.75. For example, an initial R1 increase of 1.57 ± 0.01 1/s and a half time of 1.73 ± 0.02 h were observed in a healthy human subject (male, 32 years 96 kg) with the same technique after intravenous application of a single dose of Gd-DTPA (Magnevist®, Bayer Schering, unpublished data). The dose-related R1 increase and thus the distribution volume of 0.21 l/kg were consistent with values obtained in the marmoset, but the excretion was 3.5 times slower in the human volunteer. Related to the metabolic body weight the applied doses of gadobutrol are comparable between man [0.33 mmol/kg$^{0.75}$ (96 kg body mass)] and marmoset monkey [0.25 mmol/kg$^{0.75}$ (0.51 kg body mass)].

The differences observed in T1 and MT histograms in comparison to humans likely reflect the different proportions of WM, GM and CSF spaces. As expected, the quantitative T1 values were shorter than those determined for 7T (Bock et al., 2011) but similar to those in humans at 3T (Table 2). The T1 mode between those of WM and GM was not observed at 7T, probably due to partial volume averaging. However, the origin of the intermediate T1 signals was consistent with the difference between the histograms of whole brain and cerebellum shown in Fig. 4 of Liu et al. (2011). The values of the MT saturation obtained in the marmosets were also similar to human brain (Gringel et al., 2009). Automated methods for voxel-based quantification have been developed for multi-parameter mapping in humans (Draganski et al., 2011) and can be transferred to marmosets. At the same magnetic field strength, an improved comparability of preclinical animal models and clinical studies in humans can be expected. The notable exception is the effective transverse relaxation rate, R2*. The deep brain nuclei, in particular the globus pallidus and the caudate nucleus, showed smaller R2* values than in humans (Helms and Dechent, 2009) indicating a lower iron content in marmosets. This was consistent with slightly longer T1 times observed in marmosets and with the absence of the typical strong hypointensity of the globus pallidus in T2-w MRI (not shown). The reproducibility of R2* in the ventral regions of the marmoset brain may be not as good as in humans, due to the influence of susceptibility-related B0 inhomogeneities. These affect a disproportionally larger area of marmoset brain and may be the main reason for the degradation of the EPI signals, compromising SNR and leading to spatial distortions. Like EPI-based DTI, R2* mapping would benefit from improved routines for local shimming.

The distinct contrast of the acute inflammatory lesion in WM reflects the underlying changes of tissue microstructure. A longitudinal EAE study of marmosets monitored a similar set of contrast parameters as proposed in the 30 min protocol (Blezer et al., 2007). For the study of animal models involving acute inflammatory processes, the application of contrast agent can be combined with a prolongation of anesthesia by ketamine.

In the healthy animals used in the current study, we presented potential applications for T1 mapping (blood concentration of paramagnetic contrast agent), R2* mapping (endogeneous iron deposits) and MT mapping (cortical parcellation). Also in humans, cortical areas have recently been successfully identified using R1 mapping based on multi-echo FLASH MRI (Sereno et al., in press). Focusing on area V5, we demonstrated the applicability of color-coded overlays of parameter maps as a supplement to histogram analysis. In addition to T1, the FLASH-based multi-parameter protocol yielded the MT saturation, which represents an improved semi-quantitative parameter for MT as compared to the MT ratio

(Helms et al., 2008a,b). This study added evidence for the superior sensitivity of the MT saturation to axonal density in GM. Contrary to T1 maps, the MT saturation maps are not biased by tissue iron content and local flip angle inhomogeneities. However, these sources of error were less prominent than in humans (Helms et al., 2008b). Local variation of the flip angle can be ruled out because the common marmoset is considerably smaller than the RF wavelength at 3T.

5. Conclusion

We demonstrate that structural neuroimaging of the common marmoset can be performed using a 3T whole body MRI system within the time constraints of injection anesthesia. Intracortical structures can be resolved at an isotropic resolution of 0.33 mm with a standard wrist coil. We exclusively used commercial clinical equipment and manufacturer-provided sequences. In combination with quantitative MRI this opens the avenue for longitudinal studies of marmoset models for a number of neurological diseases without the need for a dedicated small animal MRI system.

Acknowledgements

This work was supported by the Schilling Foundation, the Center for Molecular Physiology of the Brain (CPMG), and the Center for Nanoscale Microscopy and Molecular Physiology of the Brain (CNMPG). EGR received funding from the ERA-Net "NEURON".

References

Bihel E, Pro-Sistiaga P, Letourneur A, Toutain J, Saulnier R, Insausti R, et al. Permanent or transient chronic ischemic stroke in the non-human primate: behavioral, neuroimaging, histological and immunohistochemical investigations. J Cereb Blood Flow Metab 2010;30:273–85.

Bihel E, Roussel S, Toutain J, Bernaudin M, Touzani O. Diffusion tensor MRI reveals chronic alterations in white matter despite the absence of a visible ischemic lesion on conventional MRI: a nonhuman primate study. Stroke 2011;42:1412–9.

Blezer ELA, Bauer J, Brok HPM, Nicolay K, Hart BA. Quantitative MRI-pathology correlations of brain white matter lesions developing in a non-human primate model of multiple sclerosis. NMR Biomed 2007;20:90–103.

Bock NA, Kocharyan A, Silva AC. Manganese-enhanced MRI visualizes V1 in the non-human primate visual cortex. NMR Biomed 2009;22:730–6.

Bock NA, Hashim E, Kocharyan A, Silva AC. Visualizing myeloarchitecture with magnetic resonance imaging in primates. Ann NY Acad Sci 2011;1225(Suppl. 1):E171–81.

Boretius S, Schmelting B, Watanabe T, Merkler D, Tammer R, Czeh B, et al. Monitoring of EAE onset and progression in the common marmoset monkey by sequential high-resolution 3D MRI. NMR Biomed 2006;19:41–9.

Constantinides CD, Atalar E, McVeigh ER. Signal-to-noise measurements in magnitude images from NMR phased arrays. Magn Reson Med 1997;38:852–7.

Dathe H, Helms G. Exact algebraization of the signal equation of spoiled gradient echo MRI. Phys Med Biol 2010;55:4231–45.

Diem R, Demmer I, Boretius S, Merkler D, Schmelting B, Williams SK, et al. Autoimmune optic neuritis in the common marmoset monkey: Comparison of visual evoked potentials with MRI and histopathology. Invest Ophthalmol Vis Sci 2008;49:3707–14.

Draganski B, Ashburner J, Hutton C, Kherif F, Frackowiak RSJ, Helms G, et al. Regional specificity of MRI contrast parameter changes in normal ageing revealed by voxel-based quantification (VBQ). Neuroimage 2011;55:1423–34.

Garea-Rodríguez E, Schlumbohm C, Czéh B, König J, Helms G, Heckmann C, et al. Visualizing dopamine transporter integrity with iodine-123-FP-CIT SPECT in combination with high resolution MRI in the brain of the common marmoset monkey. J Neurosci Methods 2012;210:195–201.

Gringel T, Schulz-Schaeffer WJ, Elolf E, Frölich A, Dechent P, Helms G. Optimized high-resolution mapping of magnetization transfer (MT) at 3 Tesla for direct visualization of substructures of the human thalamus in clinically feasible measurement time. J Magn Reson Imaging 2009;29:1285–92.

Helms G, Dechent P. Increased SNR and reduced distortions by averaging multiple gradient echo signals in 3D FLASH imaging of the human brain at 3 T. J Magn Reson Imaging 2009;29:198–204.

Helms G, Dathe H, Dechent P. Quantitative FLASH MRI at 3 T using a rational approximation of the Ernst equation. Magn Reson Med 2008a;59:667–72.

Helms G, Dathe H, Kallenberg K, Dechent P. High-resolution maps of magnetization transfer with inherent correction for RF inhomogeneity and T1 relaxation obtained from 3D FLASH MRI. Magn Reson Med 2008b;60:1396–407.

Helms G, Draganski B, Frackowiak R, Ashburner J, Weiskopf N. Improved segmentation of deep brain grey matter structures using magnetization transfer (MT) parameter maps. Neuroimage 2009;47:194–8.

Hikishima K, Quallo MM, Komaki Y, Yamada M, Kawai K, Momoshima S, et al. Population-averaged standard template brain atlas for the common marmoset (*Callithrix jacchus*). Neuroimage 2011;54:2741–9.

Jack Jr CJ, Bernstein MA, Fox NC, Thompson P, Alexander G, Harvey D, et al. The Alzheimer's disease neuroimaging initiative (ADNI): MRI methods. J Magn Reson Imaging 2008;27:685–91.

Kirik D, Annett LE, Burger C, Muzyczka N, Mandel RJ, Björklund A. Nigrostriatal alpha-synucleinopathy induced by viral vector-mediated overexpression of human alpha-synuclein: a new primate model. Proc Natl Acad Sci USA 2003;100:2884–9.

Liu JV, Bock NA, Silva AC. Rapid high-resolution three-dimensional mapping of T(1) and age-dependent variations in the non-human primate brain using magnetization-prepared rapid gradient-echo (MPRAGE) sequence. Neuroimage 2011;56:1154–63.

Merkler D, Ernsting T, Kerschensteiner M, Brück W, Stadelmann C. A new focal EAE model of cortical demyelination: multiple sclerosis-like lesions with rapid resolution of inflammation and extensive remyelination. Brain 2006a;129:1972–83.

Merkler D, Schmelting B, Czeh B, Fuchs E, Brück W, Stadelmann C. Myelin oligodendrocyte glycoprotein-induced experimental autoimmune encephalomyelitis in the common marmoset reflects the immunopathology of pattern II multiple sclerosis lesions. Mult Scler 2006b;12:369–74.

Palazzi X, Bordier N. The marmoset brain in stereotaxic coordinates. New York: Spinger; 2008.

Pintaske J, Martirosian P, Graf H, Erb G, Lodemann KP, Claussen CD, et al. Relaxivity of gadopentate dimeglumine (Magnevist), gadobutrol (Gadovist), and gadobenate (MultiHance) in human blood plasma at 0.2, 1.5, and 3 Tesla. Invest Radiol 2006;41:213–21.

Sati P, Silva AC, van Gelderen P, Gaitan MI, Wohler JE, Jacobson S, et al. In vivo quantification of T(2)* anisotropy in white matter fibers in marmoset monkeys. Neuroimage 2012;59:979–85.

Sereno MI, Lutti A, Weiskopf N, Dick F. Mapping the human cortical surface by combining quantitative T1 with retinotopy. Cereb Cortex, in press.

Tofts P, editor. Quantitative MRI of the brain. Chichester, UK: Wiley; 2005.

van Vliet SAM, Blezer ELA, Jongsma MJ, Vanwersch RA, Olivier B, Philippens IH. Exploring the neuroprotective effects of modafinil in a marmoset Parkinson model with immunohistochemistry, magnetic resonance imaging and spectroscopy. Brain Res 2008;1189:219–28.

Yamada M, Momoshima S, Masutani Y, Fujiyoshi K, Abe O, Nakamura M, et al. Diffusion-tensor neuronal fiber tractography and manganese-enhanced MR imaging of primate visual pathway in the common marmoset: preliminary results. Radiology 2008;249:855–64.

Yuasa S, Nakamura K, Kohsaka S. Stereotaxic atlas of the marmoset brain: vol. 2. Immunohistochemical plates and MR images National Institute of Neuroscience. Tokyo, Japan: National Center of Neurology and Psychiatry; 2010.